Nonclassical nonlinear elasticity of crystalline structures

Aakash Khandelwal ![ORCID] and Sunil Kishore Chakrapani ![ORCID][*]

Department of Mechanical Engineering, Michigan State University, East Lansing, Michigan 48824, USA

Hysteretic elastic nonlinearity has been shown to result in a dynamic nonlinear response which deviates from the known classical nonlinear response; hence this phenomenon was termed nonclassical nonlinearity. Metallic structures, which typically exhibit weak nonlinearity, are typically categorized as classical nonlinear materials. This article presents a material model which derives stress amplitude dependent nonlinearity and damping from the mesoscale dislocation pinning and breakaway to show that the lattice defects in crystalline structures can give rise to nonclassical nonlinearity. The dynamic nonlinearity arising from dislocations was evaluated using resonant frequency shift and higher order harmonic scaling. The results show that the model can capture the nonlinear dynamic response across the three stress ranges: linear, classical nonlinear, and nonclassical nonlinear. Additionally, the model also predicts that the amplitude dependent damping can introduce a softening-hardening nonlinear response. The present model can be generalized to accommodate a wide range of lattice defects to further explain nonclassical nonlinearity of crystalline structures.

I. INTRODUCTION

Elastic nonlinearity in materials has been of interest to researchers in a wide range of disciplines including materials science, engineering, and geophysics. Naturally, this would mean the bulk nonlinear response would be a result of tangled contributions from a wide variety of lattice and higher scale defects. Of particular interest are the contributions from the mesoscale defects since they contribute directly to macro or bulk scale elasticity, and nanoelasticity. Typically, the bulk nonlinearity has been characterized using phenomenological models for different types of materials including crystalline, amorphous, polymeric, rubber, etc. Specifically for crystalline metallic structures, a hyperelastic stress-strain relationship with a Taylor series expansion of the strain energy density has been used [1–3]:

$$\varphi = \tfrac{1}{2}C_{ijkl}\varepsilon_{ij}\varepsilon_{kl} + \tfrac{1}{6}C_{ijklmn}\varepsilon_{ij}\varepsilon_{kl}\varepsilon_{mn} + \cdots, \qquad (1)$$

where ε_{ij} are the Lagrangian strain components, C_{ijkl} are the linear second order Brugger elastic coefficients, and C_{ijklmn} are the nonlinear third order Brugger elastic coefficients [4,5]. Equation (1) accommodates the anisotropy of the elastic constants as well. These nonlinear elastic constants can also be determined theoretically using empirical force-constant models, molecular-dynamics simulations, and density function theory (DFT) methods [6]. There is also a large body of work which covers measurement of the nonlinear elastic constants using static methods [7] and dynamic methods, such as nonlinear wave propagation [4,8], acoustoelastic waves [9], and nonlinear resonances [10].

Recent work in the past two decades has demonstrated a new type of nonlinearity that arises from the microstructure. It exhibits anomalous nonlinear dynamic behavior such as hysteretic damping, nonlinearity, discrete memory, and slow dynamics [11–15]. Since these stress amplitude and time dependent behaviors are not classical characteristics of nonlinear materials, this was termed "nonclassical nonlinearity" (NCNL). NCNL materials have been reported to exhibit different behavior based on the applied stress range [16,17]: (a) linear elastic, which is a low stress amplitude range where the structure behaves like a linear elastic material due to low contributions of nonlinearity [11]; (b) classical nonlinear (CNL), where the elasticity is controlled by classical definitions of nonlinearity prescribed by Landau and Lifshitz [18]; and finally (c) nonclassical nonlinear, where the elasticity is controlled by mesoscale features. Any NCNL structure will exhibit all three stress ranges [11,16,17]. However, the stress value at transition between the different stress regimes is dependent on the hysteretic mechanisms. Furthermore, at low stress amplitudes, the hysteretic response is low, so it exhibits an apparent linear and CNL response. While there is a wide body of literature which explores the NCNL response of geomaterials [19], concrete [20], reinforced composite structures [10,21,22], and granular materials [23,24], there are only a few articles which explore the NCNL behavior of metallic structures [14,25–29]. This presents an interesting challenge since the source of NCNL behavior in metallic structures has not been well understood. There is no work in the literature which has explored the influence of lattice defects on the bulk NCNL behavior of metallic structures.

The general approach towards understanding nonclassical nonlinearity has been to use phenomenological models which model the hysteretic nonlinear material behavior. While most of the present work modifies the bulk phenomenological coefficients to fit the experimentally observed response, the

---

[*]Also at Department of Electrical and Computer Engineering, Michigan State University, East Lansing, Michigan 48824, USA; csk@egr.msu.edu
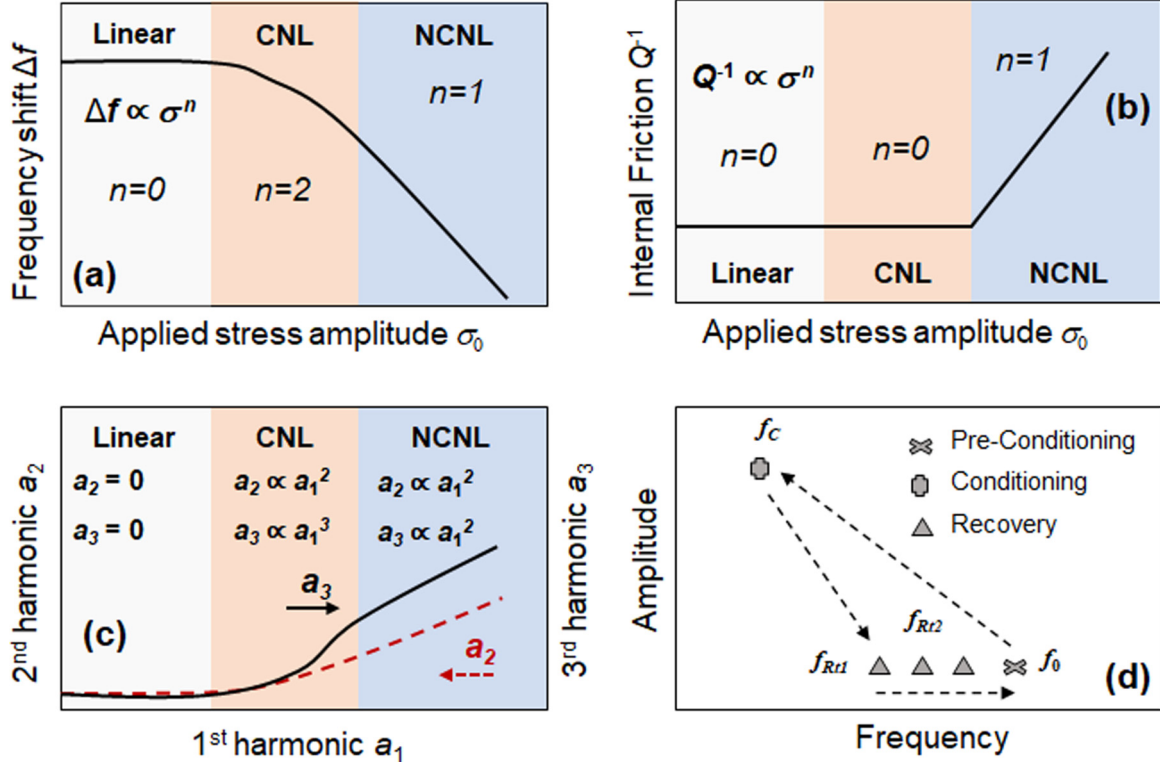
FIG. 1. Schematic showing the nonclassical nonlinear behavior of structures. For each parameter such as frequency shift, internal friction, and harmonic scaling, the three strain ranges, linear, classic nonlinear (CNL), and nonclassical nonlinear (NCNL), are shown. (a) The frequency shift $\Delta f \propto \sigma^n$, where n can take up values of 0, 1, or 2. (b) The nonlinear internal friction $Q^{-1} \propto \sigma^n$, where n can take up values of 0 or 1. (c) The higher order harmonic amplitude scaling laws with fundamental harmonic: $a_x \propto a_1^n$, where $x = 2$ for second order harmonic, $x = 3$ for third order harmonic, and the power law term n can take up the values 0, 2, or 3. (d) Slow dynamic showing the preconditioning frequency (f_0), the high amplitude conditioning frequency (f_c), and the recovery frequency over time (f_{Rti}) at time t_i.

physical effects are lost in the process. Presently there is no physical model which can capture all three stress regions. The objective of this article is to use physical effects such as dislocation dynamics to explain the nonclassical nonlinearity and damping observed in crystalline structures. Previous experiments show that dislocations can result in a linear frequency shift [30], but the exact mechanisms have not been explained. The present work uses dislocation dynamics in a resonant bar experiment to show that the overall elastic behavior will be nonclassical nonlinear in nature. The dislocation based model captures the nonlinearity in the three stress ranges and the transitions between them. Additionally interesting phenomena such as softening-hardening nonlinearity are also shown.

II. BACKGROUND

The NCNL behavior typically arises due to the hysteretic nonlinear elasticity. This has been traditionally modeled using a stress-strain relationship given by [31]

$$\sigma = \int [K_0(1 - \beta\varepsilon(t) - \delta\varepsilon(t)^2$$
$$- \chi(\Delta\varepsilon + \varepsilon(t)\text{sign}(\dot{\varepsilon}))) + \cdots] d\varepsilon, \quad (2)$$

where K_0 is the linear second order elastic stiffness, β and δ are the third and fourth order nonlinearity parameters, and χ is the hysteretic parameter, which is strain rate dependent. A

resonant beam with this material law will exhibit the following characteristics:

(1) *Nonlinear frequency shift.* In the case of linear elastic materials, with increase in stress amplitude, the resonant frequency of the beam remains constant; $\Delta f \propto \sigma^0$. For CNL materials, a quadratic decrease in resonant frequency is observed with increasing stress amplitude, as prescribed by Landau [18]: $\Delta f \propto \sigma^2$. But for NCNL materials, a linear frequency shift is observed: $\Delta f \propto \sigma$ as shown in Fig. 1(a). By definition, this dynamic response is strain amplitude dependent, i.e., a NCNL material will exhibit all three stress regions, and a CNL material will only exhibit the linear and CNL regions.

(2) *Nonlinear internal friction.* The internal friction (Q^{-1}) remains constant with stress amplitude for linear and CNL materials, $Q^{-1} \propto \sigma^0$, and increases linearly for NCNL materials, $Q^{-1} \propto \sigma$, as shown in Fig. 1(b).

(3) *Higher order harmonic scaling.* The higher order harmonics are defined as, i.e., $f_2 = 2 \times f_1$, $f_3 = 3 \times f_1$, where f_1 is the fundamental harmonic, and f_2 and f_3 are the second and third order harmonic frequencies, and a_2 and a_3 are their respective amplitudes. For linear materials, there are no higher order harmonics, i.e., $a_2, a_3 = 0$. In the case of CNL materials, $a_2 \propto a_1^2$, and $a_3 \propto a_1^3$. For NCNL materials, $a_3 \propto a_1^2$ as shown in Fig. 1(c). Once again, this will be an amplitude dependent behavior, and NCNL materials will exhibit all three characteristics.
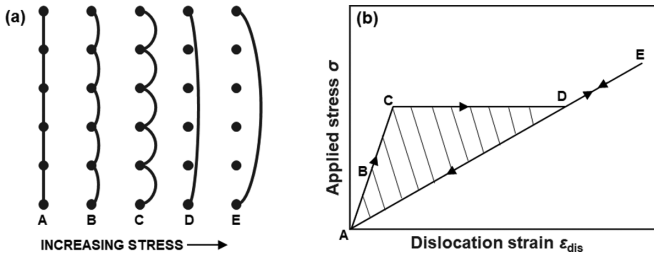
FIG. 2. Schematic showing (a) the dislocation breakaway process as a function of stress and (b) the resulting stress-strain plot.

(4) *Slow dynamics.* Slow dynamics occur in purely NCNL materials, and are not found in linear or CNL materials. If the high stress amplitude is sustained over a period of time (conditioning) and removed, the resonant frequency does not recover to the original (unconditioned) value immediately; rather it slowly recovers over time to its original value as shown in Fig. 1(d). This has been categorized as a multirelaxation phenomenon [32] and probed using a combination of different techniques [27].

Existing NCNL models have focused on an array of microcracks or hysteretic mesoscopic units (HMUs) [23] which can open and close over a stress cycle to simulate hysteretic nonlinearity as shown in Eq. (2). The development of the Preisach-Mayergoyz (PM) space model has tremendously helped to explain the nonclassical phenomenon. Since hysteresis is central to NCNL response, the PM space model works well for structures like rocks and concrete, which might have an array of cracks. However, physically, not all structures contain such an assembly of microcracks. In metallic structures, the hysteretic effects can arise from the lattice defects [14,25,26,33]. Therefore, modeling the microstructural response for crystalline materials would help in developing a deeper understanding of NCNL behavior.

Lattice defects such as precipitates and dislocations have been shown to be sources of nonlinearity and internal friction in metals [34,35]. Dislocation motion under the action of an applied harmonic stress is the most prominent source of hysteretic nonlinearity [35,36]. Explorations in this area gave rise to the idea of amplitude dependent internal friction (ADIF) [37–39]. The Koehler-Granato-Lücke model [35] provided the first comprehensive explanation of frequency dependent mechanical damping due to dislocation motion in a viscous medium (prominent only in the megahertz range), and stress amplitude dependent damping due to dislocation bowing and breakaway for stress waves propagating through a crystal lattice. The Koehler-Granato-Lücke model assumes that the crystal lattice contains a network of dislocations pinned down by impurity particles, with the dislocation loop length L_C defined as the length of the dislocation line between the weak pinning points and the network length L_N composed by a series of weakly pinned loop lengths between the strong pinning points, as shown in Fig. 2(a). The dislocation line undergoes hysteretic behavior as it is subjected to an applied harmonic stress.

During the increasing quarter cycle of stress, an undeformed dislocation loop L_C bows, and continues to do so until the breakaway stress is reached, as shown in Fig. 2. During

this stage, the modulus of the dislocation stress-strain curve is governed by the length L_C. Once the breakaway stress is achieved, the dislocation unpins catastrophically from the weak pinning points, causing a sharp increase in the dislocation strain for no increase in the stress. Further increases in the stress correspond to a bowing of the dislocation network line L_N, with the modulus of the dislocation stress-strain curve now being governed by L_N. During the decreasing quarter cycle, the unpinned dislocation line L_N collapses elastically obeying the modulus determined by L_N until it reaches its undeformed configuration, when it is once again pinned by the impurity particles. The result is a hysteretic stress-strain loop, with the energy loss proportional to the area enclosed by the same. This hysteretic behavior leads to a stress amplitude dependent loss, which has been characterized by Granato and Lücke for propagating stress waves in the crystals [Eq. (13)].

The formulations from the Granato-Lücke model have been used for propagating waves, but have not been studied in the context of a resonant system. Additionally, there is no work in the literature which has explored the effect of dislocation breakaway on the nonlinear response. The combined effect of dislocation dynamics influenced nonlinearity and damping on the frequency shift and higher order harmonic characteristics is also currently unknown. The present work aims to fill these gaps and determine if dislocation dynamics can give rise to dynamic elastic behavior which can be classified as nonclassical nonlinearity.

III. MODEL

Our approach to modeling the nonclassical behavior starts with introducing stress amplitude dependent nonlinearity and damping arising as a result of the hysteretic dislocation dynamic model of Koehler, Granato, and Lücke [35]. Scaling the mesoscale response to the macroscopic response requires the use of dynamic vibration models. Coupling the mesoscale and the macroscale models allows us to capture the dislocation dynamic effects in the macroscopic vibration model.

A. Modeling dislocation behavior

Granato and Lücke had assumed an exponential distribution of loop lengths in the initial lattice, which changes as the material is stressed, and the breakaway process proceeds. For a dislocation line, breakaway occurs when the force exerted by a dislocation line on a weak pinning point exceeds the binding force given by Cottrell's theory. For a maximum binding force f_m, we define a "breakaway length" $\mathcal{L}$, given by [35]

$$\mathcal{L} = \frac{\pi f_m}{4bR\sigma_{\text{app}}}, \tag{3}$$

where σ_{app} is the instantaneous value of the applied stress. The other parameters in Eq. (3) can be found in Table I. The values of the parameters correspond to Fe, but can be generalized for any crystalline solid. For a harmonic loading condition, as is considered in the present work, σ_{app} is given by

$$\sigma_{\text{app}} = \sigma_0 \sin \Omega t, \tag{4}$$

where σ_0 is the applied stress amplitude and is proportional to the applied force. Breakaway occurs only when L_N

TABLE I. Descriptions and values of parameters used in the model. The values for parameters correspond to iron.

Symbol	Description	Value (unit)
ρ_0	Material density	7850 (kg m^{-3})
C_{11}	Second order elastic constant	205 (GPa)
M_{111}	Third order elastic constant	-2400 (GPa)
G	Shear modulus	80 (GPa)
η^e	Elastic Kelvin-Voigt damping	4753 (Pa s)
ν	Poisson's ratio	0.29
L_C	Dislocation loop length	0.27 (μm)
L_N	Dislocation network length	$10L_C$
b	Burger's vector	0.3 (nm)
Λ	Dislocation density	10^{12} (m^{-2})
R	Schmid factor	0.3
ζ	Shear to longitudinal strain constant	10
σ_1	Initial (biasing) stress	0.02 (MPa)
C	Force per unit length in a bowed-out dislocation	$\frac{2Gb^2}{\pi(1-\nu)}$
f_m	Maximum binding force on dislocation line	1.0448×10^{-9} (N)
	Parameters for NL beam model	
L	Length of beam	76.2 (mm)
W	Width of beam	19.05 (mm)
h	Thickness of beam	7.29 (mm)

exceeds $\mathcal{L}$. $\mathcal{L}$ is a function of the instantaneous applied stress σ_{app}, as evident from Eq. (3), and varies over the course of a harmonic stress cycle. We may compute the value of $\mathcal{L}$ over an increasing quarter cycle of stress to identify if and when catastrophic breakaway of the dislocation line occurs. Of course, no dislocation breakaway occurs at low stress amplitudes, and it is only the length L_C which bows, and recovers during the decreasing quarter cycle. As the stress amplitude increases, breakaway occurs increasingly sooner in the increasing quarter cycle of stress, and the dislocation length L_C bows and breaks away, after which the length L_N bows. The dislocation line of length L_N collapses during the decreasing quarter cycle, and repins when the stress drops to zero.

To integrate the effects of dislocation breakaway into a material model, we assume a nonlinear stress-strain relationship which has previously been considered in the literature [4,5,30,34,40,41] given by

$$\sigma_{ij} = C_{ijkl}\varepsilon_{kl} + M_{ijklmn}\varepsilon_{kl}\varepsilon_{mn}, \tag{5}$$

where C_{ijkl} are the second order elastic constants (SOECs), and M_{ijklmn} are the third order elastic constants (TOECs), related to the Brugger elastic coefficients as

$$M_{ijklmn} = \tfrac{1}{2}(C_{jlmn}\delta_{ik} + C_{ijnl}\delta_{km} + C_{jknl}\delta_{im} + C_{ijklmn}), \tag{6}$$

where δ_{ij} are Kronecker deltas.

To include the effect of damping, we will also introduce a Kelvin-Voigt damping term into the stress-strain response. Using Voigt notation to contract the elastic constants, and restricting ourselves to one dimension along the solid, allows us to rewrite the stress-strain relationship as

$$\sigma_{xx} = C_{11}\varepsilon_{xx} + M_{111}\varepsilon_{xx}^2 + \eta\dot{\varepsilon}_{xx}, \tag{7}$$

where $\eta\dot{\varepsilon}_{xx}$ is the Kelvin-Voigt damping term to account for the material damping. The elastic nonlinearity parameter

arising purely from lattice is defined by [42]

$$\beta^e = -\frac{M_{111}}{C_{11}}. \tag{8}$$

In addition to lattice contribution (β^e), there is also a dislocation contribution to the nonlinearity parameter, first described by Hikata *et al.* [34], which will be discussed in the following section.

1. Stress amplitude dependent nonlinearity

The existence of a biasing stress σ_1 leads to a dislocation contribution to the nonlinearity parameter, which for a dislocation loop of length $2L$ is given by [34]

$$\beta^d = \frac{12}{5}\frac{\zeta R^3 \Lambda C_{11}^2 L^4 \sigma_1}{G^3 b^2}. \tag{9}$$

For a dislocation line that has not broken away, $2L = L_C$, and for one that has, $2L = L_N$. The corresponding values of β^d for the two cases, called β_C^d and β_N^d, respectively, may be found simply by substituting the appropriate value of L into Eq. (9). It must be noted that there exists a distribution of loop lengths in the lattice, and the calculation of β^d is based on average loop lengths.

If the applied stress amplitude is too small to trigger dislocation breakaway, i.e., $\mathcal{L} > L_N$ over the complete stress cycle, we have

$$\beta^d = \beta_C^d. \tag{10}$$

If the applied stress amplitude is large enough to cause dislocation breakaway, we can find the time instant $\mathcal{T}$ during the increasing quarter cycle at which this occurs by equating $\mathcal{L}$ and L_N. Strictly speaking, $\mathcal{T}$ depends on the forcing frequency Ω. This dependence, however, is found to be very small; we ignore it and use Eq. (3) to compute $\mathcal{L}$, and consequently $\mathcal{T}$, at

the resonant frequency ω. We use $\mathcal{T}$ to find the proportion of time, P, a dislocation line spends unpinned during the increasing quarter cycle. Furthermore, if breakaway has occurred, the dislocation line remains unpinned over the entire decreasing quarter cycle, repinning when the stress drops to zero. β^d is therefore a time dependent parameter. We disregard its time dependence and compute an average value of β^d from its variation over a half cycle, given by

$$\beta^d = \tfrac{1}{2}\big[(1 - P)\beta_C^d + (1 + P)Q\beta_N^d\big], \tag{11}$$

where Q is a factor between zero and 1 that accounts for the probability of a dislocation breaking away to the average length L_N based on multiple slip plane orientations. The overall nonlinearity parameter β is found simply by summing the value of β^e found from Eq. (8) with the value of β^d from either Eq. (10) (if breakaway does not occur) or Eq. (11) (if breakaway occurs):

$$\beta = \beta^e + \beta^d. \tag{12}$$

2. Stress amplitude dependent damping

Considering the exponential distribution of dislocation loop lengths, Granato and Lücke have estimated a value of $\mathcal{L}$ at which the stress-dislocation strain relationship becomes nonlinear, and provided the stress-dislocation strain relation for the increasing and decreasing stress quarter cycles [35].

The energy lost per cycle due to the dislocation bowing and breakaway, ΔW, is found by computing the area enclosed. The stress-dislocation strain curve and the stress amplitude dependent dislocation decrement are finally expressed as [35]

$$\Delta^d = \frac{\Delta W}{2W} = \frac{T \Delta_0 \Lambda L_N^3}{\pi L_C} \frac{\Gamma}{R \sigma_0} \exp\left(\frac{-\Gamma}{R \sigma_0}\right), \tag{13}$$

where T is the orientation factor accounting for multiple slip plane orientations [35], and Δ_0 is given by

$$\Delta_0 = \frac{8 C_{11} b^2}{\pi^3 C}, \tag{14}$$

and Γ is the effective dislocation modulus given by

$$\Gamma = \frac{\pi f_m}{4 b L_C}. \tag{15}$$

The decrement arising from dislocations is further used to compute the dislocation damping, which when combined with the damping from the lattice gives the damping parameter of the system.

B. Dynamic model

The phenomenon of NCNL in crystalline solids is studied within the framework of a nonlinear beam vibration model. The dynamic model for the flexural vibration of a cantilever beam is derived beginning from the Kirchhoff plate theory, with the in-plane and transverse midplane displacements given by

$$u(x, y, z, t) = u_0(x, y, t) - z \frac{\partial w}{\partial x}, \tag{16}$$

$$w(x, y, z, t) = w_0(x, y, t), \tag{17}$$

where t is the time. The resulting linear von Kármán strain-displacement relationship (with the nonlinear contribution being neglected) with the x-direction strain is given by

$$\varepsilon_{xx} = \frac{\partial u_0}{\partial x} - z \frac{\partial^2 w_0}{\partial x^2}. \tag{18}$$

The dynamic equation is derived in a manner analogous to previous work [10]. Details of the derivation are presented in Appendix A. We drop the term in $q\dot{q}$ from Eq. (A14) for simplicity, and assume a harmonic external forcing given by $F \sin(\Omega t)$ to write the final dynamic equation as

$$\ddot{q} + \omega^2 q + \phi q^2 + \gamma q^3 + \alpha \dot{q} = F \sin(\Omega t). \tag{19}$$

The parameters in Eq. (19) are defined in Eqs. (A15)–(A18).

We now account for the amplitude dependence of the nonlinearity and damping due to dislocation breakaway within the dynamic model to express the nonlinearities ϕ and γ, and the damping α as amplitude dependent parameters.

We use Eq. (12) to rewrite the expressions for ϕ and γ in Eqs. (A16) and (A17), as

$$\phi = \frac{B_{11}}{\Delta_I} \int_0^L p(p'')^2 dx - \frac{1}{\Delta_I} \int_{-h/2}^{h/2} (\beta^e + \beta^d) C_{11} z^3 dz \int_0^L p[p'' p^{IV} + (p''')^2] dx, \tag{20}$$

$$\gamma = -\frac{1}{\Delta_I} \int_{-h/2}^{h/2} (\beta^e + \beta^d) C_{11} z^2 dz \int_0^L p(p'')^3 dx, \tag{21}$$

where Δ_I is given by Eq. (A20).

The effect of dislocation damping cannot be incorporated into the material model [Eq. (7)] directly. We therefore compare the value of the dislocation decrement Δ^d from Eq. (13) to the decrement Δ for the nonlinear oscillator from Eq. (19), found from its first order solution and given in Eq. (34). We equate Δ and Δ^d, and solve for the damping parameter due to dislocation motion, termed α^d. Equations (A12) and (A18) may then be used to back-calculate the Kelvin-Voigt dislocation damping parameter η^d that would lead to α^d. We

write the Kelvin-Voigt damping parameter due to both lattice and dislocation contributions as

$$\eta = \eta^e + \eta^d. \tag{22}$$

The damping parameter α, defined in Eq. (A18), can now be rewritten, accounting for amplitude dependent dislocation effects as

$$\alpha = \frac{1}{\Delta_I} \int_{-h/2}^{h/2} (\eta^e + \eta^d) z^2 dz \int_0^L p(p^{IV}) dx, \tag{23}$$

where Δ_I is given by Eq. (A20).

Equation (19) is solved using the method of multiple time scales (MTS) [43]. Two time scales are used to express the temporal function as

$$q(t, \epsilon) = q_0(T_0, T_1) + \epsilon q_1(T_0, T_1) + \cdots, \qquad (24)$$

where $T_0 = t$ and $T_1 = \epsilon t$. This allows the transformation of the time derivatives, which are then given by

$$\frac{d}{dt} = D_0 + \epsilon D_1, \qquad (25)$$

$$\frac{d^2}{dt^2} = D_0^2 + 2\epsilon D_0 D_1 + \cdots, \qquad (26)$$

where $D_n = \partial/\partial T_n$.

1. Primary resonances and decrement of the nonlinear oscillator

The primary resonances arise when the excitation frequency is close to the linear resonant frequency, i.e., $\Omega \approx \omega$. A detuning parameter ς is used to show this nearness as

$$\Omega = \omega + \epsilon\varsigma. \qquad (27)$$

The primary resonances are excited with relatively small forcing amplitudes, and the MTS solution thus assumes the nonlinearities, the damping, and the forcing to be of the scale ϵ, allowing us to rewrite Eq. (19) as

$$\ddot{q} + \omega^2 q + \epsilon\phi q^2 + \epsilon\gamma q^3 + \epsilon\alpha\dot{q} = \epsilon F \sin(\omega T_0 + \varsigma T_1), \qquad (28)$$

where Eq. (27) has been used to rewrite Ωt.

The subsequent steps in the MTS solution are provided in Appendix B 1. Squaring and adding Eqs. (B9) and (B10) gives us the frequency response for primary resonance,

$$\left(\frac{1}{2}a\alpha\right)^2 + \left(a\varsigma - \frac{3}{8}\frac{a^3\gamma}{\omega}\right)^2 = \frac{F^2}{4\omega^2}. \qquad (29)$$

The calculation of the decrement of the nonlinear oscillator (19) requires us to compare the energy lost per cycle to the maximum energy stored in the oscillator. The instantaneous energy stored in the oscillator is represented by

$$E = \underbrace{\frac{1}{2}\dot{q}^2}_{\text{Kinetic}} + \underbrace{\frac{1}{2}\omega^2 q^2 + \frac{1}{4}\gamma q^4}_{\text{Potential}}, \qquad (30)$$

where q is taken to be the solution of the ϵ^0 order equation (B1), q_0, given in Eq. (B3). Using Eqs. (B5) and (B6) and simplifying, we may write

$$q = \frac{1}{2}ae^{i(\Omega t - \theta)} + \frac{1}{2}ae^{-i(\Omega t - \theta)}. \qquad (31)$$

$\dot{q}$ is obtained from a simple time derivative of the above expression. Substituting the expressions for q and $\dot{q}$ into Eq. (30) allows us to solve for the *maximum* energy stored in the system, finally obtained as

$$E_{\max} = \frac{1}{2}\omega^2 a^2 + \frac{1}{4}\gamma a^4. \qquad (32)$$

The energy lost per cycle can be found by integrating the product of the instantaneous forcing and the velocity $\dot{q}$ with respect to the time t over one time period. This loss is represented by

$$\Delta E = \int_0^{2\pi/\Omega} F \sin(\Omega t)\dot{q}\,dt = -\pi a F \cos\theta. \qquad (33)$$

The expression for the decrement of the nonlinear oscillator is now given by

$$\Delta = \frac{\Delta E}{2E_{\max}} = \frac{-\pi a F \cos\theta}{a\omega^2 + \frac{1}{2}a^3\gamma}, \qquad (34)$$

for which we obtain $\cos\theta$ from Eqs. (B9) and (B10), and a *in terms of* α from Eq. (29). Equation (34) indicates that Δ depends on the forcing frequency Ω in addition to the forcing and the system parameters. However, this frequency dependence is found to be negligible, and restricts the application of Eq. (34) to the resonant frequency ω.

We finally derive from Eq. (29) an expression for the resonant frequency shift, by evaluating the detuning parameter at the peak amplitude, where $da/d\varsigma = 0$. The expression for the frequency shift of the primary resonance is given by

$$\varsigma_p = \frac{3}{8}\frac{F^2\gamma}{\alpha^2\omega^3}, \qquad (35)$$

which predicts a quadratic softening frequency shift with the forcing amplitude F if all other parameters remain constant. The resonant frequency at any forcing value is given simply by the sum $\omega + \varsigma_p$.

2. Higher order harmonic resonances

Higher order harmonics arise at integer multiples of the excitation frequency, i.e., $n\Omega$, where $n = 1, 2, 3, \ldots$ due to the nonlinear interactions. For propagating waves, the definition of higher order harmonics is straightforward, i.e., second order harmonic frequency $f_2 = 2f_1$ and third order harmonic $f_3 = 3f_1$. However, for resonant vibrations, higher order harmonics are defined based on the vibration mode. If the fundamental resonance is excited at a resonant mode, a corresponding resonant mode at the higher order harmonic frequency is necessary to observe the nonlinear coupling. However, this requirement is only satisfied for torsional modes, and does not hold for flexural modes. Therefore, to observe the nonlinear coupling to excite a higher order harmonic of order n for flexural modes, we need to provide the harmonic excitation near ω/n to ensure that the nonlinear coupling will result in a higher order harmonic near ω. This also means that nonresonant excitation requires the forcing amplitudes to be large, i.e., of the order ϵ^0. The equation of motion for corresponding the MTS solution is now written as

$$\ddot{q} + \omega^2 q + \epsilon\phi q^2 + \epsilon\gamma q^3 + \epsilon\alpha\dot{q} = F \sin(\Omega T_0). \qquad (36)$$

The second order harmonic arises when Ω is near $\omega/2$. The detuning parameter ς for this case is given by

$$2\Omega = \omega + \epsilon\varsigma. \qquad (37)$$

The details of the MTS solution for higher order harmonic resonance, starting from Eq. (36), is given in Appendix B 2. Squaring and adding Eqs. (B17) and (B18) gives the expression for the frequency response as

$$\left(\frac{1}{2}a_2\alpha\right)^2 + \left(a_2\varsigma - \frac{3}{8}\frac{a_2^3\gamma}{\omega} - 3\frac{a_2\gamma\Xi^2}{\omega}\right)^2 = \frac{\phi^2\Xi^4}{\omega^2}. \qquad (38)$$

It must be noted that the quadratic nonlinearity ϕq^2 contributes only to the frequency response of the second order harmonic, Eq. (38). ϕ does not appear in Eqs. (29) and (40),
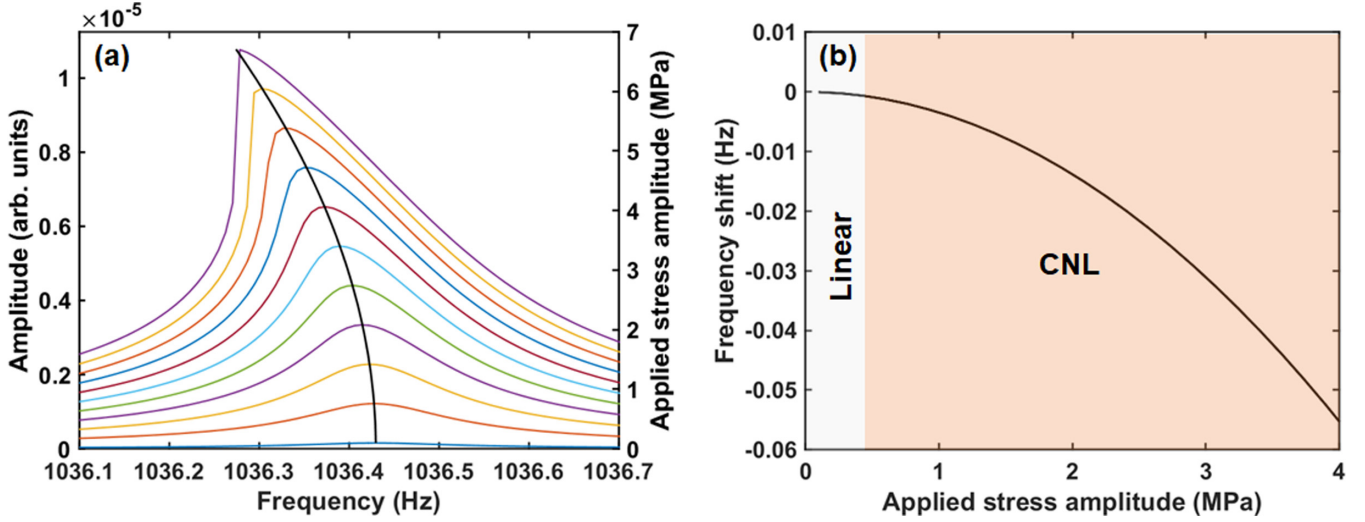
FIG. 3. (a) Frequency response curves for the primary resonance, developed with constant values of the nonlinearity parameter β and the damping parameter α, showing CNL behavior, i.e., quadratic softening of the resonant frequency with the applied stress amplitude σ_0. (b) Frequency shift with the applied stress amplitude σ_0, showing a brief region with almost zero frequency shift, followed by a region with quadratic softening; this combined shift is referred to as CNL in subsequent results.

and has no influence on the frequency responses of the primary resonance or the third order harmonic.

Similar to the second order harmonic, the third order harmonic arises when the forcing frequency Ω is near $\omega/3$. The detuning parameter ς is now defined as

$$3\Omega = \omega + \epsilon\varsigma. \tag{39}$$

The frequency response is derived by squaring and adding Eqs. (B22) and (B23). The resulting expression is

$$\left(\frac{1}{2}a_3\alpha\right)^2 + \left(a_3\varsigma - \frac{3}{8}\frac{a_3^3\gamma}{\omega} - 3\frac{a_3\gamma\Xi^2}{\omega}\right)^2 = \frac{\gamma^2\Xi^6}{\omega^2}. \tag{40}$$

Unlike the explicit quadratic relationship between frequency shift and applied stress for the fundamental frequency given by Eq. (35), the higher order harmonics do not have an explicit relationship. Equations (38) and (40) need to be evaluated numerically to understand the harmonic amplitude dependence on the fundamental excitation amplitude.

IV. RESULTS

A. Classical nonlinear behavior

The frequency response equation given by Eq. (29) allows us to develop the resonance curves to understand the dynamic behavior of the structure. By definition of Eq. (35), a quadratic softening frequency shift is expected. At very low applied stress amplitudes, the frequency shift will be infinitesimally small, i.e., ~ 0, and as the applied stress amplitude increases, a quadratic shift in the frequency will be observed. Therefore, as long as the coefficients of the equation of motion, Eq. (19), are not dependent on the applied stress amplitude, classical nonlinear behavior is expected. In the present work, CNL behavior is observed on disregarding all dislocation effects, i.e., setting η^d and β^d to zero, such that only lattice contributions to the nonlinearity and the damping are considered. The resulting frequency shift of the primary resonance is quadratic

with the forcing amplitude F, and by extension, the applied stress amplitude σ_0, as predicted by Eq. (35) and shown in Fig. 3. As shown in Fig. 3, the classical model can capture both the linear and the classical nonlinear zones.

In addition to the nonlinear frequency shift, higher order harmonics can be used to characterize the material response. A linear material will not exhibit higher order harmonics, while a CNL material will exhibit higher order harmonics which scale with fundamental amplitude. The second order harmonic will scale quadratically ($a_2 \propto a_1^2$), and the third order harmonic will scale cubically ($a_3 \propto a_1^3$) with fundamental amplitude. The frequency response equations for the second and third order harmonics, given by Eqs. (38) and (40), were evaluated for increasing fundamental excitation amplitude, and the resulting higher order harmonic peak amplitudes were captured. For ease of presentation, rather than fitting with a quadratic or cubic functions, we plot a_2 against a_1^2 and a_3 against a_1^3, both of which are supposed to show linear dependencies for CNL behavior. Figures 4(a) and 4(b) show a quadratic and cubic scaling of the second and third order harmonics, which is consistent with CNL behavior.

B. Influence of stress amplitude dependent nonlinearity

We consider the nonlinearity parameter to be given by Eq. (12), which in turn influences the values of ϕ and γ, as in Eqs. (20) and (21), while assuming a constant damping coefficient, i.e., $\eta = \eta^e$. When the applied stress amplitude is below the threshold to trigger dislocation breakaway, the dislocation contribution to the nonlinearity parameter is given by Eq. (10), which is small compared to the value of β^e for the value of σ_1 considered. Furthermore, the value of β in this range is not significantly different from that considered for the CNL case. When the applied stress amplitude exceeds the dislocation breakaway threshold, the dislocation contribution to the nonlinearity parameter is given by Eq. (11), and a sharp increase in its value can be observed, which stabilizes
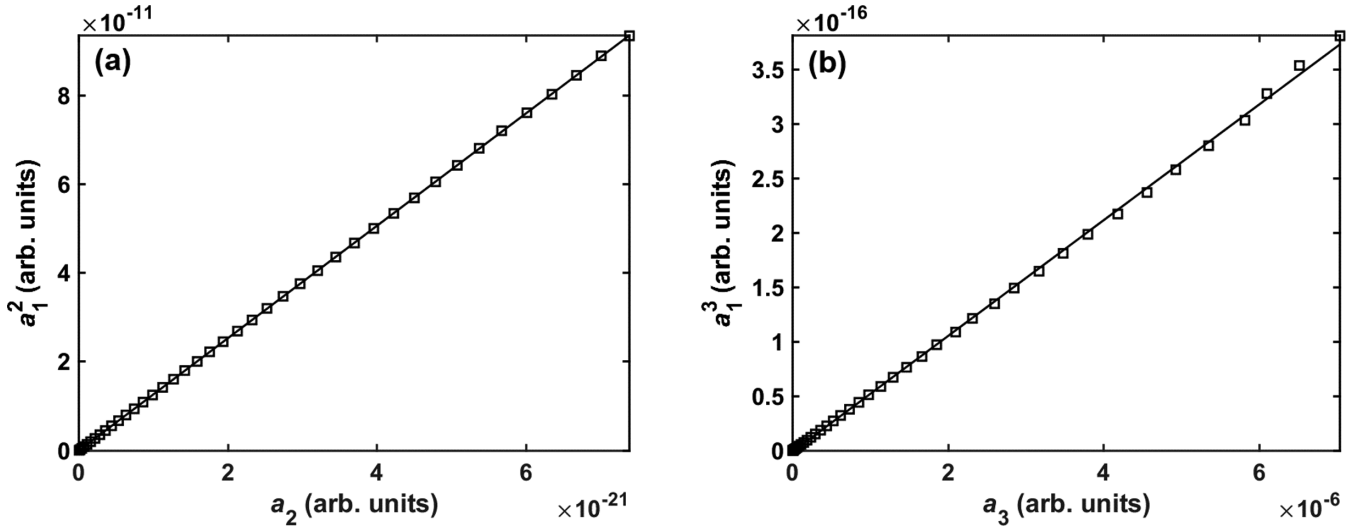
FIG. 4. Higher order harmonic scaling for CNL behavior. (a) Second order harmonic amplitude a_2 scaling with the corresponding fundamental harmonic amplitude a_1; $a_2 \propto a_1^2$. (b) Third order harmonic amplitude a_3 scaling with the corresponding fundamental harmonic amplitude a_1; $a_3 \propto a_1^3$.

at higher applied stress amplitudes. This variation of β with the applied stress amplitude due to breakaway is shown in Fig. 5(a) for different choices of the breakaway probability Q. Larger increases in β are observed for larger values of Q. The stress amplitude dependence of β is expected to cause a deviation in the frequency shift of the fundamental harmonic. Figure 5(b) shows the frequency shift of the primary resonance with the applied stress amplitude, derived using Eq. (35), for the different variations in β. The response clearly shows the existence of two regions, one where β is constant, and another above $\sim$3 MPa, where β starts varying due to breakaway. Similar behavior has been shown experimentally for aluminum by Cantrell and Yost [44,45]. Interestingly, both regions show a quadratic frequency shift behavior.

We now look at how the breakaway process affects the higher order harmonics. Since there are many breakaway probabilities Q, we choose a value at which a considerable change in β can be observed: $Q = 0.3$. We proceed as described in the previous section to find the dependence of a_2 and a_3 on a_1. For the range of the applied stress amplitude where β remains constant, a_2 scales linearly with a_1^2, and a_3 scales linearly with a_1^3, as was the case for CNL behavior; this is shown in Fig. 6. Interestingly, in the breakaway region, a_2 still scales quadratically with a_1, albeit with a small change in the slope as shown in Fig. 6(a). However, a_3 begins to scale with a_1^2 in the postbreakaway region, which is characteristic of NCNL materials rather than CNL behavior. As can be seen in Fig. 6(b) the scaling is not uniform in the NCNL range owing
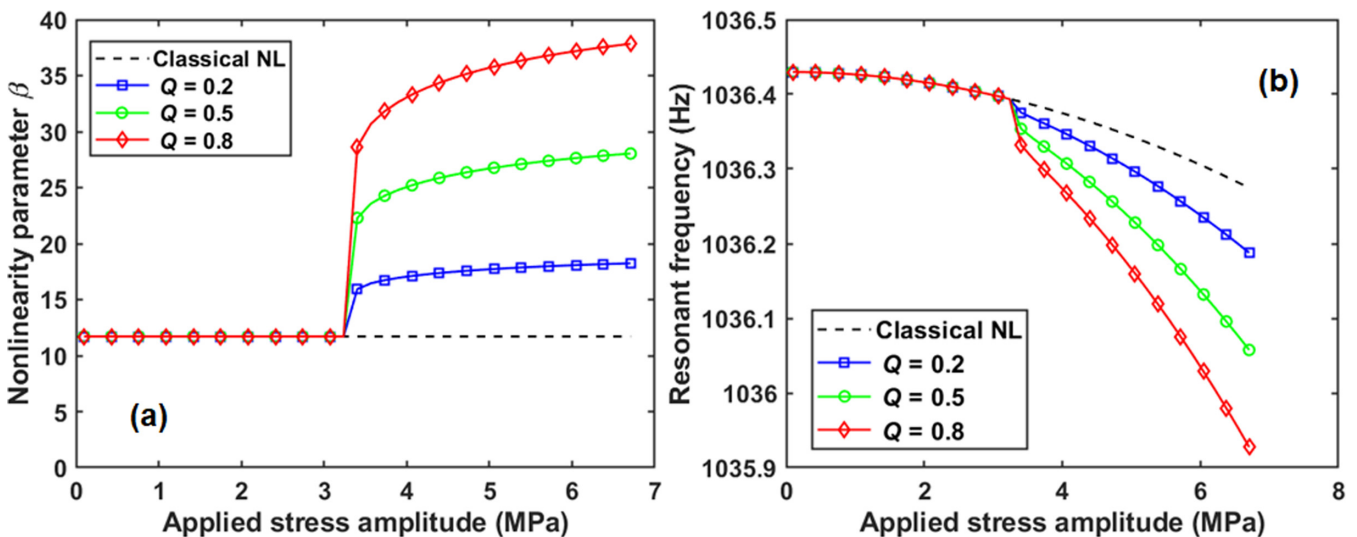

FIG. 5. (a) Variation of the nonlinearity parameter β with the applied stress amplitude σ_0 for different choices of the breakaway probability Q. (b) Frequency shift of the primary resonance with the applied stress amplitude σ_0 for different variations in β corresponding to different breakaway probabilities Q.
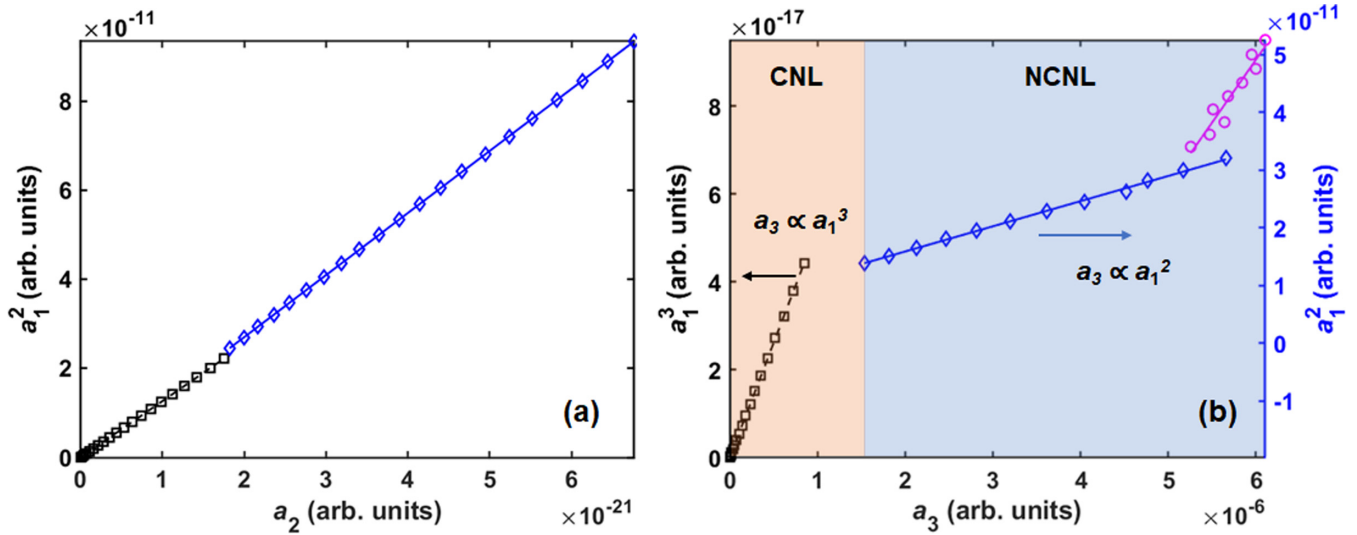
FIG. 6. Higher order harmonic scaling for variable β obtained for $Q = 0.3$. (a) Second order harmonic amplitude a_2 scales quadratically with fundamental harmonic amplitude a_1; $a_2 \propto a_1^2$ over the entire range of β. (b) Third order harmonic amplitude a_3 scaling with fundamental harmonic amplitude a_1; $a_3 \propto a_1^3$ in the CNL region, and $a_3 \propto a_1^2$ in the NCNL region. The black squares represent response before breakaway, and blue diamond markers represent after breakaway. The data shown in pink circles were noisy and could not be fit with either a_1^3 or a_1^2.

to the variable rate of increase in β with σ_0 shown previously. Two separate fits in the NCNL range are thus developed.

C. Influence of stress amplitude dependent damping

We now consider the effect of stress dependent damping by setting the damping parameter, α, to have a dislocation contribution, as given by Eq. (23). We further set the nonlinearity parameter to have no dislocation contribution, i.e., $\beta = \beta^e$. The dislocation contribution to α is only prominent beyond applied stress amplitudes sufficient to cause dislocation breakaway; the resulting α therefore remains constant until a certain value of applied stress amplitude, after which it increases with the applied stress amplitude. Figure 7(a) shows the dependence of α on the applied stress amplitude

for different values of the orientation factor T. The rate of the increase in α is higher at larger values of T, as evident from Fig. 7(a).

The stress amplitude dependence of α is expected to cause a deviation in the frequency shift of the primary resonance from the quadratic nature, typical of CNL systems. Figure 7(b) shows the frequency shift of the primary resonance with the applied stress amplitude, derived following Eq. (35) for different rates of increase in α. We note that the case for which T is set to 4.8×10^{-4} shows a *rightward* frequency shift at elevated values of σ_0. This softening-hardening behavior is intriguing and will be discussed later.

We again look at how the higher order harmonics scale, setting $T = 1.2 \times 10^{-4}$ and proceeding as described in Sec. IV A. For the range of the applied stress amplitude where
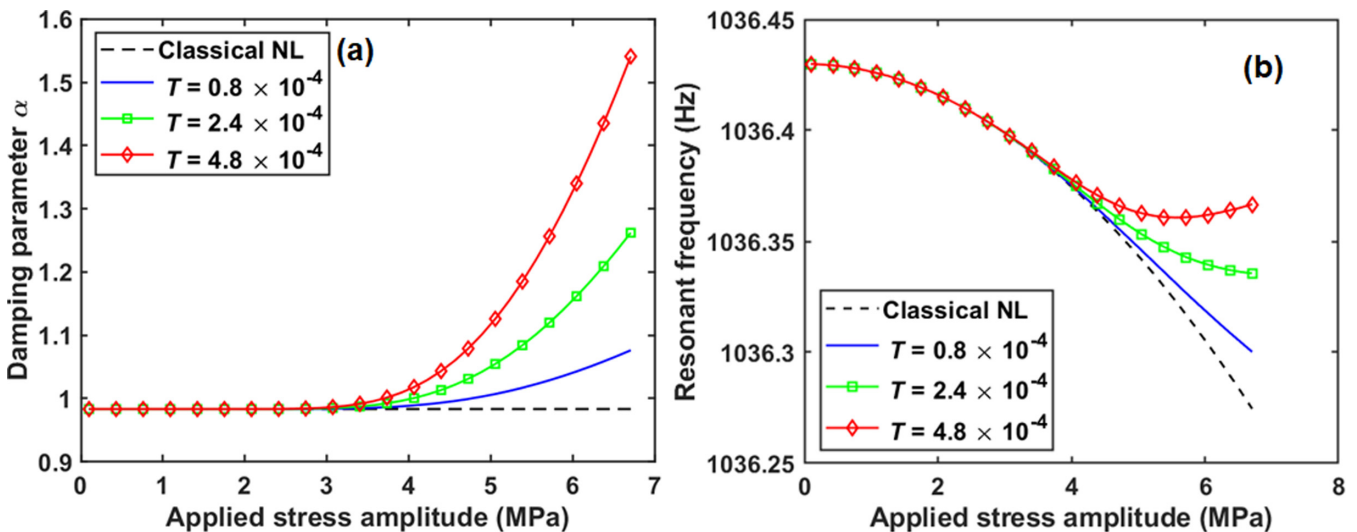

FIG. 7. (a) Variation of the damping parameter α with the applied stress amplitude σ_0 for different values of the orientation factor T. (b) Frequency shift of the primary resonance with the applied stress amplitude σ_0 for different rates of increase in α corresponding to different orientation factors T.
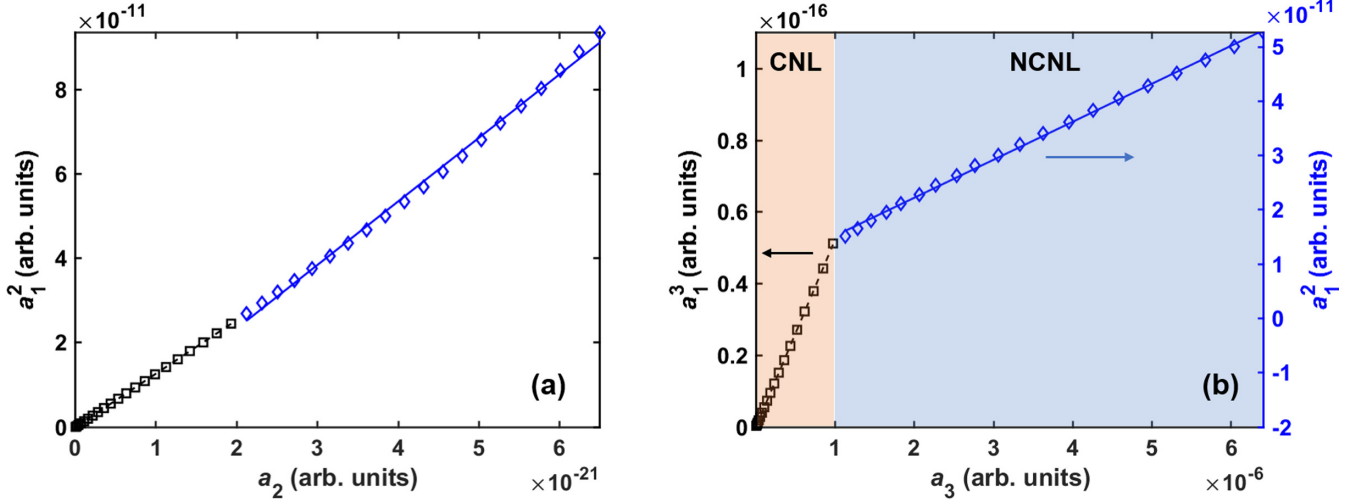
FIG. 8. Higher order harmonic scaling for variable α obtained for $T = 1.2 \times 10^{-4}$. (a) Second order harmonic amplitude a_2 scaling with the corresponding fundamental harmonic amplitude a_1; $a_2 \propto a_1^2$ over the entire range of α. (b) Third order harmonic amplitude a_3 scaling with the corresponding fundamental harmonic amplitude a_1; $a_3 \propto a_1^3$ as long as α remains constant (CNL region), and $a_3 \propto a_1^2$ when α increases (NCNL region). The black squares represent response before breakaway, and blue diamond markers represent after breakaway.

α remains constant, $a_2 \propto a_1^2$, and $a_3 \propto a_1^3$, as for CNL behavior. Once α starts increasing with the applied stress amplitude, these scaling laws are no longer valid. While a_2 now scales reasonably linearly with a_1^2, albeit with a rate different from the one followed previously [Fig. 8(a)], a_3 now scales linearly with a_1^2. The two distinct regions in the scaling of a_3 are shown in Fig. 8(b).

D. Combined effect of stress amplitude dependent damping and nonlinearity

We now consider the combined effect of stress amplitude dependent nonlinearity and damping, using Eqs. (12), (20), (21), and (23) to describe the coefficients of the dynamic equation (19). The variations of β and α follow the same trend as in Figs. 5(a) and 7(a). Different combinations of Q and T are used to derive curves for the frequency shift of the primary resonance as shown in Fig. 9. The frequency shift is quadratic as long as β and α remain constant which signifies a CNL behavior. But this deviates at higher applied stress amplitudes to an apparent linear frequency shift with and without hardening effects, which signifies NCNL characteristics.

The higher order harmonic behavior for combined variation in β and α was obtained by setting $Q = 0.3$ and $T = 1.2 \times 10^{-4}$. As long as β and α remain constant, we observe CNL behavior, with a_2 scaling linearly with a_1^2, and a_3 scaling linearly with a_1^3. Once the parameters start increasing, a_3 once again starts scaling proportional to a_1^2, while a_2 is still proportional to a_1^2, which once again points towards NCNL behavior. Beyond a certain applied stress value, the response becomes noisy and does not fit well with quadratic or cubic fits. We have denoted these by the pink circle symbols in Fig. 10(b).

V. DISCUSSIONS

In Figs. 5(b) and 9 we observe a small sudden transition region in the frequency shift. This seems like an anomalous

region which is typically not reported in experimental results. We believe this arises from the nonlinearity due to the breakaway. According to the Granato-Lücke model, beyond breakaway, we have a large increase in loop length, which results in hysteresis and nonlinearity. The threshold stress for this breakaway is instantaneous and once this stress value is attained, the dislocation unpins and the loop length increases to network length. We believe this anomalous region is a result of the sudden increase in loop length. We assume that the dislocation unpins instantly, which results in sudden increase of the nonlinearity parameter as shown in Fig. 5(a). This argument is supported by the fact that if we only consider nonlinear damping, α, then we do not see this anomalous region (Fig. 7). If we, however, assume a more progressive unpinning action, then this region could possibly disappear. On the other hand, a more realistic solution will be to consider a statistical distribution of dislocation characteristics. The breakaway length from the Granato-Lücke model considers an average length based on the distribution. If, however, we consider a statistical distribution of breakaway lengths, and solve the current model for this distribution, we might get a smoother curve, which will be closer to what is typically observed for NCNL materials. Such a statistical distribution has been explored by several authors with good success [28,46,47]. As mentioned earlier, the transition between CNL and NCNL might not happen at a distinct stress value. This transition stress depends on the scale at which we evaluate the response, i.e., at very small length scales, the transition stress might be distinct due to the smaller distribution of break-away lengths, whereas at bulk scales, a larger statistical ensemble might give a distribution of breakaway lengths, which can give us a distribution of transition stresses and an overall smoother transition. The statistical approach might also provide us with more physical insights on the transition between the different stress ranges. This will be explored in future works.

NCNL behavior of metallic structures has been barely explored in the literature. Metallic and crystalline structures
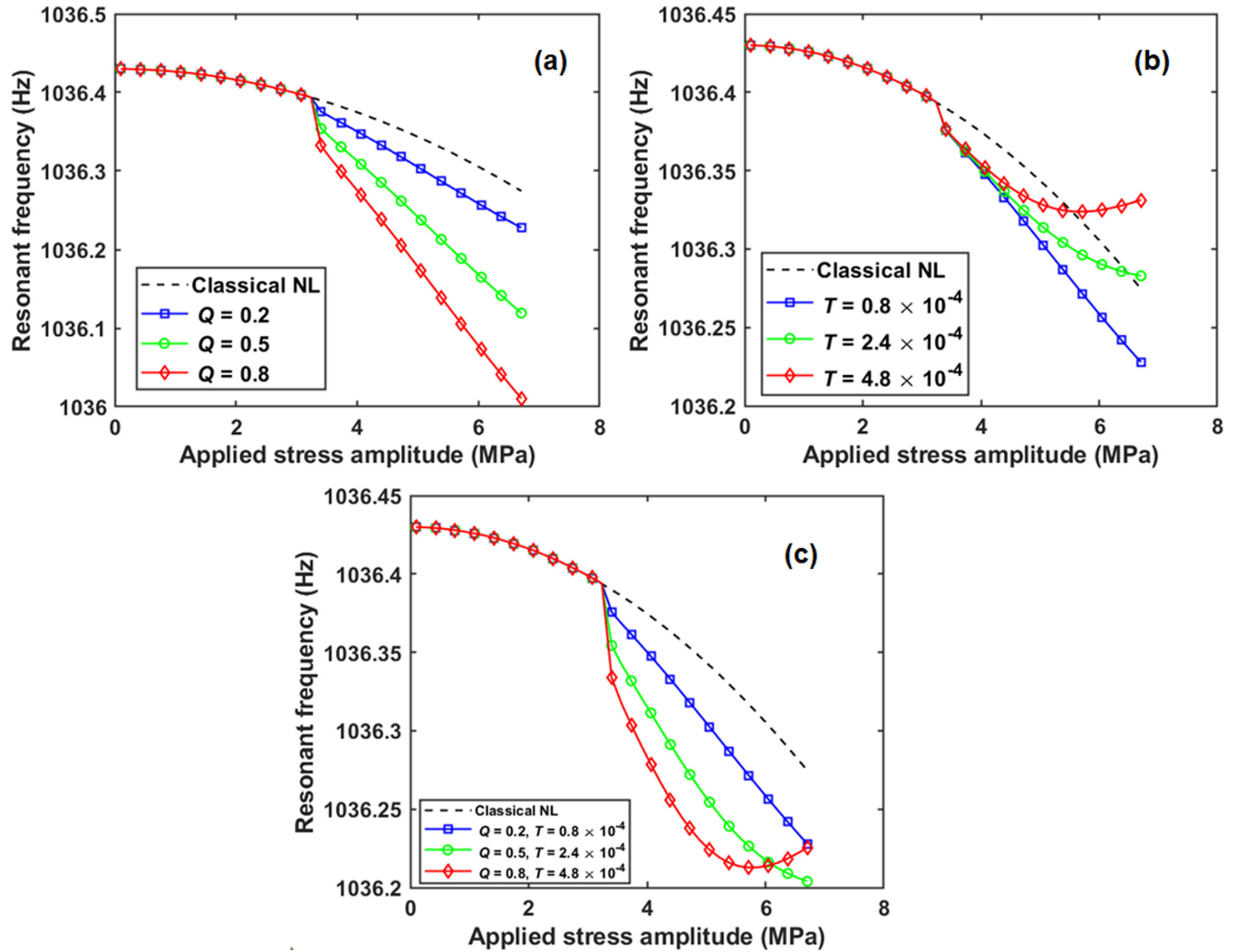
FIG. 9. Frequency shift of the primary resonance with the applied stress amplitude σ_0 for (a) $T = 0.8 \times 10^{-4}$, with variable Q, showing a linear frequency shift in the NCNL region, (b) $Q = 0.2$, with variable T, showing hardening behavior for elevated values of T in the NCNL region, and (c) simultaneous increases in Q and T. Larger values of Q correspond to larger frequency shifts, while larger values of T correspond to more pronounced hardening, and smaller effective frequency shifts.

typically exhibit low levels of nonlinearity ($\beta = 5$–20) and have been sidelined compared to geomaterials which are typically three to four orders of magnitude more nonlinear ($\beta = 10^3$) [12]. Due to their low nonlinearity, metallic structures have been typically categorized as classical nonlinear materials. While there are several previous works which have reported experimental results for NCNL behavior of metallic structures [25,30,48–51], by far, there has been no physics based model to explain this behavior in metals. The results from Sec. IV show that accounting for dislocation dynamics allows us to model the NCNL behavior and categorized metallic structures as nonclassical nonlinearity. More importantly, the model presented here shows that the apparent NCNL behavior can be captured without the use of an explicit hysteretic function as given by Eq. (2). This explicit form and the PM space model have become a staple in explaining the NCNL behavior for geomaterials. However, the present work demonstrates that the same effect can be accomplished by accounting for stress amplitude dependent coefficients. In other words, from a macro or bulk phenomenological perspective,

the frequency shift behavior is controlled by coefficients of Eq. (19). By introducing a stress amplitude dependence on the coefficients, i.e., $\phi(\sigma_0)$, $\gamma(\sigma_0)$, and $\alpha(\sigma_0)$, the apparent frequency shift becomes dependent on the applied stress. This can result in apparent frequency shifts which can take up any power law, i.e., linear, quadratic, or any real value. We use the term apparent to describe the frequency shift since it is not explicit like the CNL response, which has a quadratic relationship with applied stress given by Eq. (29).

While the present model accurately captures three of four characteristics of NCNL materials, it cannot capture slow dynamics by itself. We believe this model needs updated coefficients which become functions of relaxation time. Since this would require a deeper investigation, we prefer to explore this as a stand-alone work. Other authors have also explored this approach with good success [52]. The present model could also be used to verify experimental observations by fitting the dislocation coefficients. However, an extensive study will be required to validate the dislocation characteristics. The current model will also accommodate three-dimensional experimental
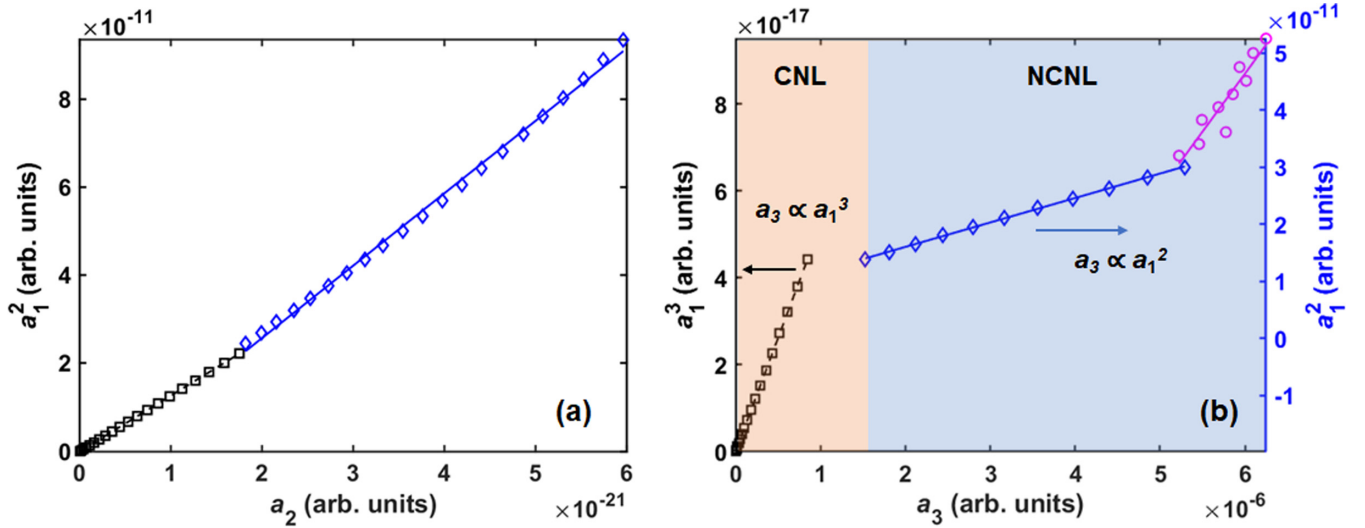
FIG. 10. Higher order harmonic scaling for combined variations in β and α obtained for $Q = 0.3$ and $T = 1.2 \times 10^{-4}$. (a) Second order harmonic amplitude a_2 scaling with the corresponding fundamental harmonic amplitude a_1; $a_2 \propto a_1^2$ over the entire range. (b) Third order harmonic amplitude a_3 scaling with the corresponding fundamental harmonic amplitude a_1; $a_3 \propto a_1^3$ as long as the parameters remain constant (CNL region), and $a_3 \propto a_1^2$ when the parameters increase as described (NCNL region). The black squares represent response before breakaway, and blue diamond markers represent after breakaway. The data shown in pink circles were noisy and could not be fit with either a_1^3 or a_1^2.

setups as long as the first order flexural mode is chosen as demonstrated earlier [10]. The model can further be modified for specific modes and displacements.

While the model presented here uses lattice defects for a crystalline structure, it can be easily extended to geomaterials which also have crystalline grains. Previous studies show us that the geomaterials have hysteretic bonds [23] connecting the larger crystalline structures. The nonlinearity arising from these bonds will be much larger than the nonlinearity within the crystalline structure. This raises an interesting question: What can be classified as NCNL behavior? By definition, any behavior which deviates away from CNL behavior can be classified as NCNL. For example, previous experimental results on the influence of dislocations show a sinusoidal behavior in the resonance frequency shift [30]. Furthermore, the influence of "Buck hook" behavior, once again results in an "apparent" NCNL behavior. This was also successfully modeled using dislocation dynamics [30]. The focus of most of the research in NCNL behavior has been limited to power law scaling which uses integer values. Similar to the frequency shift, the higher order harmonic scaling laws need to be revisited for different physical phenomena for a wide category of NCNL behavior.

VI. SUMMARY AND CONCLUSIONS

The current work presents a physical model to capture non-classical nonlinearity of metallic and crystalline structures. The model's dynamic response was evaluated by coupling the dislocation model to a resonant system. The resulting meso-macroscale model manages to capture all three characteristics of NCNL materials: (i) linear frequency softening, (ii) increase in internal friction, and (iii) quadratic third order harmonic scaling with fundamental harmonic. Furthermore,

this model is an instance where all three strain ranges of a NCNL material, i.e., linear, classical nonlinear, and nonclassical nonlinear, have been captured using a single physics based model. The stress amplitude dependent coefficients point towards different scaling laws which can be a function of applied stress and the physical phenomenon. The model presented here can be further modified for different types of lattice defects and other physical features spread over multiple length scales to capture the NCNL behavior.

APPENDIX A: DERIVATION OF THE DYNAMIC EQUATION

We begin with the extended Hamilton principle,

$$\delta \int_0^t (K - \Pi + W_{nc})dt = 0, \tag{A1}$$

where K is the kinetic energy, Π is the potential energy, and W_{nc} is the work done by nonconservative forces. The potential energy can be rewritten as $\Pi = U + V$, where U is the elastic strain energy and V is the potential energy change from conservative external forces. The resulting equations of motion take the form [53]

$$\frac{\partial N_{xx}}{\partial x} = I_0 \frac{\partial^2 u_0}{\partial t^2}, \tag{A2}$$

$$\frac{\partial}{\partial x}\left(N_{xx}\frac{\partial w_0}{\partial x}\right) + \frac{\partial^2 M_{xx}}{\partial x^2} + F = I_0 \frac{\partial^2 w_0}{\partial t^2}, \tag{A3}$$

where N_{xx} and M_{xx} are the force and moment resultants, respectively; F is the externally applied force; and I_0 is the mass moment of inertia, derived from the density ρ_0 of the material. These quantities take the form

$$N_{xx} = \int_{-h/2}^{h/2} \sigma_{xx} dz, \tag{A4}$$

$$M_{xx} = \int_{-h/2}^{h/2} \sigma_{xx} z \, dz, \tag{A5}$$

$$I_0 = \int_{-h/2}^{h/2} \rho_0 dz. \tag{A6}$$

Rewriting the strain-displacement relationship, Eq. (18), in simpler notation, with primes denoting partial differentiation with respect to x,

$$\varepsilon_{xx} = u_0' - z w_0''. \tag{A7}$$

Using Eq. (A7) in the stress-strain relationship, Eq. (7), and substituting the result into Eqs. (A4) and (A5) gives

$$N_{xx} = A_{11} u_0' - B_{11} w_0'' + M_1 (u_0')^2 - 2M_2 u_0' w_0''$$
$$+ M_3 (w_0'')^2 + \mu \ddot{u}_0'' - m u' \dot{w}_0'', \tag{A8}$$

$$M_{xx} = B_{11} u_0' - D_{11} w_0'' + M_2 (u_0')^2 - 2M_3 u_0' w_0''$$
$$+ M_4 (w_0'')^2 + \mu' \ddot{u}_0'' - m u'' \dot{w}_0'', \tag{A9}$$

where

$$(A_{11}, B_{11}, D_{11}) = \int_{-h/2}^{h/2} C_{11}(1, z, z^2) dz, \tag{A10}$$

$$(M_1, M_2, M_3, M_4) = \int_{-h/2}^{h/2} M_{111}(1, z, z^2, z^3) dz, \tag{A11}$$

$$(\mu, \mu', \mu'') = \int_{-h/2}^{h/2} \eta(1, z, z^2) dz. \tag{A12}$$

We simplify the derivation by neglecting the axial inertia, such that the in-plane force resultant becomes independent of x, i.e., $\partial N_{xx}/\partial x = 0$, and considering negligibly small in-plane displacements, i.e., $u_0 \approx 0$. The force and moment resultants in Eqs. (A8) and (A9) are now purely in terms of the transverse displacement w_0. We express the transverse displacement as

$$w_0(x, t) = p(x) q(t), \tag{A13}$$

where $p(x)$ corresponds to the spatial function and $q(t)$ to the temporal function. Substituting Eq. (A13) into the reduced forms of Eqs. (A8) and (A9), substituting the resulting expressions into the equation of motion (A3), simplifying, and integrating the resulting equation over the length of the beam yields the nonlinear dynamic equation

$$\ddot{q} + \omega^2 q + \phi q^2 + \gamma q^3 + \alpha \dot{q} + \kappa q \dot{q} = F, \tag{A14}$$

where

$$\omega^2 = \frac{D_{11}}{\Delta_I} \int_0^L p(p^{IV}) dx, \tag{A15}$$

$$\phi = \frac{B_{11}}{\Delta_I} \int_0^L p(p'')^2 dx + \frac{2M_4}{\Delta_I} \int_0^L p[p'' p^{IV} + (p''')^2] dx, \tag{A16}$$

$$\gamma = \frac{M_3}{\Delta_I} \int_0^L p(p'')^3 dx, \tag{A17}$$

$$\alpha = \frac{\mu''}{\Delta_I} \int_0^L p(p^{IV}) dx, \tag{A18}$$

$$\kappa = \frac{\mu'}{\Delta_I} \int_0^L p(p'')^2 dx, \tag{A19}$$

$$\Delta_I = I_0 \int_0^L p^2 dx. \tag{A20}$$

Equation (A15) defines the resonant angular frequency ω of the linear dynamic equation, Eqs. (A16) and (A17) give the coefficients of the quadratic and cubic nonlinear terms, and Eq. (A18) defines the damping parameter. The spatial function $p(x)$ is found by considering the linear vibration mode shape of a cantilever beam, and is given by

$$p(x) = \frac{1}{\sqrt{L}} \left[\cosh \frac{r_n x}{L} - \cos \frac{r_n x}{L} + m_i \left(\sinh \frac{r_n x}{L} - \sin \frac{r_n x}{L} \right) \right], \tag{A21}$$

where r_n is the nth root of the characteristic equation $1 + \cos r \cosh r = 0$, and m_i is given by

$$m_i = \frac{\cos r_n + \cosh r_n}{\sin r_n + \sinh r_n}.$$

For the current work, we consider the first order bending mode, which returns a value of 1.8751 for r_n.

APPENDIX B: DETAILS OF THE MTS SOLUTION OF THE DYNAMIC EQUATION

1. Primary resonances

Substituting Eqs. (24)–(26) into Eq. (28) and separating the coefficients of ϵ^0 and ϵ^1 returns

$$D_0^2 q_0 + \omega^2 q_0 = 0, \tag{B1}$$

$$D_0^2 q_1 + \omega^2 q_1 + 2D_0 D_1 q_0 + \phi q_0^2 + \gamma q_0^3 + \alpha D_0 q_0$$
$$= F \sin(\omega T_0 + \varsigma T_1). \tag{B2}$$

The general solution to Eq. (B1) is given by

$$q_0 = A(T_1) e^{i\omega T_0} + \bar{A}(T_1) e^{-i\omega T_0}, \tag{B3}$$

where A is an undetermined function dependent purely on T_1, and $\bar{A}$ is its complex conjugate. Substituting Eq. (B3) into Eq. (B2), and isolating the secular terms, i.e., terms in $e^{\pm i\omega t}$, which must vanish allows us to write the solvability condition as

$$2i\omega \frac{\partial A}{\partial T_1} + 3\gamma A^2 \bar{A} + i\omega \alpha A + i\frac{F}{2} e^{i\varsigma T_1} = 0. \tag{B4}$$

We express A in polar form as

$$A = \frac{1}{2} a e^{i\psi}, \tag{B5}$$

and introduce a parameter θ which enables us to transform the solvability condition to an autonomous equation, given by

$$\theta = \varsigma T_1 - \psi. \tag{B6}$$

Substituting Eqs. (B5) and (B6) into Eq. (B4) and separating the real and imaginary parts allows us to write

$$a\frac{\partial \theta}{\partial T_1} = \frac{F}{2\omega}\sin\theta + a\varsigma - \frac{3}{8}\frac{a^3\gamma}{\omega}, \tag{B7}$$

$$\frac{\partial a}{\partial T_1} = -\frac{F}{2\omega}\cos\theta - \frac{1}{2}a\alpha. \tag{B8}$$

At steady state, $\partial a/\partial T_1 = 0$ and $\partial \theta/\partial T_1 = 0$, allowing us to drop the left-hand side (LHS) from both Eqs. (B7) and (B8). Now, isolating the terms in $\sin\theta$ and $\cos\theta$ to one side of the resulting equations allows us to write

$$-\frac{F}{2\omega}\sin\theta = a\varsigma - \frac{3}{8}\frac{a^3\gamma}{\omega}, \tag{B9}$$

$$-\frac{F}{2\omega}\cos\theta = \frac{1}{2}a\alpha. \tag{B10}$$

2. Higher order harmonic resonances

Substituting Eqs. (24)–(26) into Eq. (36) and separating the coefficients of ϵ^0 and ϵ^1, as in the solution for the primary resonances, now gives

$$D_0^2 q_0 + \omega^2 q_0 = F\sin(\Omega T_0), \tag{B11}$$

$$D_0^2 q_1 + \omega^2 q_1 + 2D_0 D_1 q_0 + \phi q_0^2 + \gamma q_0^3 + \alpha D_0 q_0 = 0. \tag{B12}$$

The general solution to Eq. (B11) is given by

$$q_0 = A(T_1)e^{i\omega T_0} + i\Xi e^{-i\Omega T_0} + \bar{A}(T_1)e^{-i\omega T_0} - i\Xi e^{i\Omega T_0}, \tag{B13}$$

where A and $\bar{A}$ have the same meanings as in the previous section, and $\Xi = \frac{1}{2}F(\omega^2 - \Omega^2)^{-1}$.

a. Second order harmonic

Using the detuning parameter from Eq. (37) in Eq. (B13), substituting the resulting expression in Eq. (B12), and isolating the secular terms in $e^{i\omega t}$ allows us to write the solvability condition as

$$2i\omega\frac{\partial A}{\partial T_1} + 3\gamma A^2\bar{A} + i\omega\alpha A + 6\gamma\Xi^2 A - \phi\Xi^2 e^{i\varsigma T_1} = 0. \tag{B14}$$

Using Eqs. (B5) and (B6) in Eq. (B14), as defined in Appendix B 1, and separating the real and imaginary parts enables us to write

$$a_2\frac{\partial\theta}{\partial T_1} = \frac{\phi\Xi^2}{\omega}\cos\theta + a_2\varsigma - \frac{3}{8}\frac{a_2^3\gamma}{\omega} - 3\frac{a_2\gamma\Xi^2}{\omega}, \tag{B15}$$

$$\frac{\partial a_2}{\partial T_1} = \frac{\phi\Xi^2}{\omega}\sin\theta - \frac{1}{2}a_2\alpha. \tag{B16}$$

Again, at steady state, we drop the terms in the LHS of Eqs. (B15) and (B16) to write

$$-\frac{\phi\Xi^2}{\omega}\cos\theta = a_2\varsigma - \frac{3}{8}\frac{a_2^3\gamma}{\omega} - 3\frac{a_2\gamma\Xi^2}{\omega}, \tag{B17}$$

$$-\frac{\phi\Xi^2}{\omega}\sin\theta = -\frac{1}{2}a_2\alpha. \tag{B18}$$

b. Third order harmonic

Again, using the detuning parameter from Eq. (39) with Eqs. (B13) and (B12) and isolating the secular terms gives

$$2i\omega\frac{\partial A}{\partial T_1} + 3\gamma A^2\bar{A} + i\omega\alpha A + 6\gamma\Xi^2 A + i\gamma\Xi^3 e^{i\varsigma T_1} = 0. \tag{B19}$$

Using Eqs. (B5) and (B6) in Eq. (B19) and separating the real and imaginary parts enables us to write

$$a_3\frac{\partial\theta}{\partial T_1} = \frac{\gamma\Xi^3}{\omega}\sin\theta + a_3\varsigma - \frac{3}{8}\frac{a_3^3\gamma}{\omega} - 3\frac{a_3\gamma\Xi^2}{\omega}, \tag{B20}$$

$$\frac{\partial a_3}{\partial T_1} = -\frac{\gamma\Xi^3}{\omega}\cos\theta - \frac{1}{2}a_3\alpha. \tag{B21}$$

Again, at steady state, we drop the terms in the LHS of Eqs. (B20) and (B21) to write

$$-\frac{\gamma\Xi^3}{\omega}\sin\theta = a_3\varsigma - \frac{3}{8}\frac{a_3^3\gamma}{\omega} - 3\frac{a_3\gamma\Xi^2}{\omega}, \tag{B22}$$

$$-\frac{\gamma\Xi^3}{\omega}\cos\theta = \frac{1}{2}a_3\alpha. \tag{B23}$$

[1] Y. Hiki, Higher order elastic constants of solids, Annu. Rev. Mater. Sci. **11**, 51 (1981).

[2] A. Seeger and O. Buck, Die experimentelle ermittlung der elastischen konstanten höherer ordnung, Z. Naturforsch. A **15**, 1056 (1960).

[3] K. Huang, On the atomic theory of elasticity, Proc. R. Soc. London A **203**, 178 (1950).

[4] R. Thurston and K. Brugger, Third-order elastic constants and the velocity of small amplitude elastic waves in homogeneously stressed media, Phys. Rev. **133**, A1604 (1964).

[5] F. Birch, Finite elastic strain of cubic crystals, Phys. Rev. **71**, 809 (1947).

[6] J. Zhao, J. M. Winey, and Y. M. Gupta, First-principles calculations of second- and third-order elastic constants for single crystals of arbitrary symmetry, Phys. Rev. B **75**, 094105 (2007).

[7] T. Kroupa, V. Laš, and R. Zemčík, Improved nonlinear stress-strain relation for carbon-epoxy composites and identification of material parameters, J. Compos. Mater. **45**, 1045 (2011).

[8] D. J. Barnard, Variation of nonlinearity parameter at low fundamental amplitudes, Appl. Phys. Lett. **74**, 2447 (1999).

[9] D. S. Hughes and J. Kelly, Second-order elastic deformation of solids, Phys. Rev. **92**, 1145 (1953).

[10] S. K. Chakrapani and D. J. Barnard, Determination of acoustic nonlinearity parameter (β) using nonlinear resonance ultrasound spectroscopy: Theory and experiment, J. Acoust. Soc. Am. **141**, 919 (2017).

[11] D. Pasqualini, K. Heitmann, J. A. TenCate, S. Habib, D. Higdon, and P. A. Johnson, Nonequilibrium and nonlinear dynamics in Berea and Fontainebleau sandstones: Low-strain regime, J. Geophys. Res.: Solid Earth **112**, B01204 (2007).

[12] R. A. Guyer and P. A. Johnson, Nonlinear mesoscopic elasticity: Evidence for a new class of materials, Phys. Today **52**(4), 30 (1999).

[13] R. A. Guyer, K. R. McCall, G. N. Boitnott, L. B. Hilbert, Jr., and T. J. Plona, Quantitative implementation of Preisach-Mayergoyz space to find static and dynamic elastic moduli in rock, J. Geophys. Res.: Solid Earth **102**, 5281 (1997).

[14] P. Johnson and A. Sutin, Slow dynamics and anomalous nonlinear fast dynamics in diverse solids, J. Acoust. Soc. Am. **117**, 124 (2005).

[15] P. Johnson, *Universality of Nonclassical Nonlinearity* (Springer, Berlin, 2006), pp. 49–69.

[16] J. A. TenCate, D. Pasqualini, S. Habib, K. Heitmann, D. Higdon, and P. A. Johnson, Nonlinear and Nonequilibrium Dynamics in Geomaterials, Phys. Rev. Lett. **93**, 065501 (2004).

[17] M. Scalerandi, C. Mechri, M. Bentahar, A. Di Bella, A. S. Gliozzi, and M. Tortello, Experimental Evidence of Correlations between Conditioning and Relaxation in Hysteretic Elastic Media, Phys. Rev. Appl. **12**, 044002 (2019).

[18] L. Landau and E. Lifshitz, *Theory of Elasticity* (Pergamon, New York, 1986).

[19] R. A. Guyer, K. R. McCall, and G. N. Boitnott, Hysteresis, Discrete Memory, and Nonlinear Wave Propagation in Rock: A New Paradigm, Phys. Rev. Lett. **74**, 3491 (1995).

[20] C. Payan, T. J. Ulrich, P. Y. Le Bas, T. Saleh, and M. Guimaraes, Quantitative linear and nonlinear resonance inspection techniques and analysis for material characterization: Application to concrete thermal damage, J. Acoust. Soc. Am. **136**, 537 (2014).

[21] S. K. Chakrapani, D. J. Barnard, and V. Dayal, Influence of fiber orientation on the inherent acoustic nonlinearity in carbon fiber reinforced composites, J. Acoust. Soc. Am. **137**, 617 (2015).

[22] S. K. Chakrapani, D. J. Barnard, and V. Dayal, Influence of laminate sequence and fabric type on the inherent acoustic nonlinearity in carbon fiber reinforced composites, J. Acoust. Soc. Am. **139**, 2310 (2016).

[23] R. A. Guyer and P. A. Johnson, *Nonlinear Mesoscopic Elasticity: The Complex Behaviour of Rocks, Soil, Concrete* (Wiley, New York, 2009).

[24] M. C. Remillieux, R. A. Guyer, C. Payan, and T. J. Ulrich, Decoupling Nonclassical Nonlinear Behavior of Elastic Wave Types, Phys. Rev. Lett. **116**, 115501 (2016).

[25] M. W. Barsoum, M. Radovic, T. Zhen, P. Finkel, and S. R. Kalidindi, Dynamic Elastic Hysteretic Solids and Dislocations, Phys. Rev. Lett. **94**, 085501 (2005).

[26] T. A. Read, The internal friction of single metal crystals, Phys. Rev. **58**, 371 (1940).

[27] J. Y. Yoritomo and R. L. Weaver, Slow dynamic nonlinearity in unconsolidated glass bead packs, Phys. Rev. E **101**, 012901 (2020).

[28] C. Mechri, M. Scalerandi, and M. Bentahar, Enhancement of harmonics generation in hysteretic elastic media induced by conditioning, Commun. Nonlinear Sci. Numer. Simul. **45**, 117 (2017).

[29] M. Scalerandi, A. Gliozzi, and D. Olivero, Discrimination between cracks and recrystallization in steel using nonlinear techniques, J. Nondestruct. Eval. **33**, 269 (2014).

[30] S. K. Chakrapani, Multiscale model to study dislocation dynamics in nonlinear resonance spectroscopy of crystalline solids, Ultrasonics **96**, 220 (2019).

[31] K. E.-A. Van Den Abeele, A. Sutin, J. Carmeliet, and P. A. Johnson, Micro-damage diagnostics using nonlinear elastic wave spectroscopy (NEWS), NDT&E Int. **34**, 239 (2001).

[32] P. Shokouhi, J. Rivière, R. A. Guyer, and P. A. Johnson, Slow dynamics of consolidated granular systems: Multi-scale relaxation, Appl. Phys. Lett. **111**, 251604 (2017).

[33] A. G. Zhou, S. Basu, G. Friedman, P. Finkel, O. Yeheskel, and M. W. Barsoum, Hysteresis in kinking nonlinear elastic solids and the Preisach-Mayergoyz model, Phys. Rev. B **82**, 094105 (2010).

[34] A. Hikata, B. B. Chick, and C. Elbaum, Dislocation contribution to the second harmonic generation of ultrasonic waves, J. Appl. Phys. **36**, 229 (1965).

[35] A. Granato and K. Lücke, Theory of mechanical damping due to dislocations, J. Appl. Phys. **27**, 583 (1956).

[36] S. Asano, Theory of nonlinear damping due to dislocation hysteresis, J. Phys. Soc. Jpn. **29**, 952 (1970).

[37] G. Gremaud, The hysteretic damping mechanisms related to dislocation motion, J. Phys. Colloq. **48**, C8 (1987).

[38] G. Gremaud, 3.3 dislocation-point defect interactions, Mater. Sci. Forum **366**, 178 (2001).

[39] M. S. Blanter, I. S. Golovin, H. Neuhauser, and H. Sinning, *Internal Friction in Metallic Materials: A Handbook* (Springer, Berlin, 2007), Vol. 540.

[40] M. F. Hamilton and D. T. Blackstock (eds.), *Nonlinear Acoustics* (Academic Press, San Diego, 1998).

[41] J. H. Cantrell, Nonlinear dislocation dynamics at ultrasonic frequencies, J. Appl. Phys. **105**, 043520 (2009).

[42] J. H. Cantrell, Crystalline structure and symmetry dependence of acoustic nonlinearity parameters, J. Appl. Phys. **76**, 3372 (1994).

[43] A. Shooshtari and M. Rafiee, Nonlinear forced vibration analysis of clamped functionally graded beams, Acta Mech. **221**, 23 (2011).

[44] J. H. Cantrell and W. T. Yost, Acoustic harmonic generation and dislocation dynamics of fatigued aluminum alloys, in *Review of Progress in Quantitative Nondestructive Evaluation* (Springer, Berlin, 1993), pp. 2059–2066.

[45] J. H. Cantrell and W. T. Yost, Acoustic harmonic generation from fatigue-induced dislocation dipoles, Philos. Mag. A **69**, 315 (1994).

[46] K. E. Van Den Abeele, P. A. Johnson, R. A. Guyer, and K. R. McCall, On the quasi-analytic treatment of hysteretic nonlinear response in elastic wave propagation, J. Acoust. Soc. Am. **101**, 1885 (1997).

[47] M. Scalerandi, A. S. Gliozzi, C. L. E. Bruno, and P. Antonaci, Nonequilibrium and hysteresis in solids: Disentangling conditioning from nonlinear elasticity, Phys. Rev. B **81**, 104114 (2010).

[48] S. Maier, J.-Y. Kim, M. Forstenhäusler, J. J. Wall, and L. J. Jacobs, Noncontact nonlinear resonance ultrasound spectroscopy (NRUS) for small metallic specimens, NDT&E Int. **98**, 37 (2018).

[49] K. M. S. Levy, J.-Y. Kim, and L. J. Jacobs, Investigation of the relationship between classical and nonclassical ultrasound nonlinearity parameters and microstructural mechanisms in metals, J. Acoust. Soc. Am. **148**, 2429 (2020).

[50] C. Espinoza, D. Feliú, C. Aguilar, R. Espinoza-González, F. Lund, V. Salinas, and N. Mujica, Linear versus nonlinear acoustic probing of plasticity in metals: A quantitative assessment, Materials **11**, 2217 (2018).

[51] D. N. Fahse, K. M. S. Levy, J.-Y. Kim, and L. J. Jacobs, Comparison of changes in nonclassical (α) and classical (β) acoustic nonlinear parameters due to thermal aging of 9Cr-1Mo ferritic martensitic steel, NDT&E Int. **110**, 102226 (2020).

[52] N. Favrie, B. Lombard, and C. Payan, Fast and slow dynamics in a nonlinear elastic bar excited by longitudinal vibrations, Wave Motion **56**, 221 (2015).

[53] J. N. Reddy, *Theory and Analysis of Elastic Plates and Shells* (CRC Press, Boca Raton, FL, 2006).